Impact of β-phase in TiAl alloys on mechanical properties after high temperature air exposure

P. Sallot, Jean-Philippe P Monchoux, Sébastien Joulié, Alain Couret, M. Thomas

Impact of β-phase in TiAl alloys on mechanical properties after high temperature air exposure

P. Sallot[a], J.P. Monchoux[b,*], S. Joulié[b], A. Couret[b], M. Thomas[c]

[a] Safran Tech, Materials and Processes, Rue des Jeunes Bois, Châteaufort, 78114 Magny-Les-Hameaux, France
[b] CEMES CNRS UPR 8011, Université de Toulouse, 29 Rue Jeanne Marvig, 31055 Toulouse, France.
[c] ONERA, 29 Avenue de la Division Leclerc, 92322 Châtillon Cedex, France.

[*] To whom correspondence should be addressed: monchoux@cemes.fr

Abstract

In this paper, the influence of high temperature air exposure on the tensile properties at room temperature and on the fatigue strength at high temperature of two TiAl alloys, is studied. The alloys, Ti-48Al-2Cr-2Nb (Ti-48-2-2), and Ti-44Al-4Nb-1Mo-0.1B (TNM-B1), both exhibit near-γ microstructures, but the TNM-B1 alloy contains significant amounts of β phase. Air exposure at high temperature (650-700°C, 500 h) induces significant loss of ductility, and decrease of fatigue strength at high temperature, in the case of the β-containing TNM-B1 alloy, but not for the γ-Ti-48-2-2 alloy. This indicates a potential influence of the presence of β phase for embrittlement. Because embrittlement is believed to be the consequence of microstructure modifications in the sub-surface, first attempts have been performed to investigate these local phenomena. For this purpose, SEM, FIB, STEM-EDX and ACOM techniques have been employed. Destablilization of β and, to a lesser extent, of γ, into α_2, has been observed in the sub-surface of the TNM-B1 alloy. We interpret this as a consequence of oxygen diffusion during the high temperature air exposure, which would promote formation of α_2 phase in which oxygen solubility is high, at the expenses of the β and γ phases of lower oxygen solubility.

Keywords: A. intermetallics; B. embrittlement; B. fatigue resistance; B. Oxidation; F. electron microscopy, transmission; F. chemical map;

1. Introduction

TiAl alloys are now an industrial reality as they are currently used on the latest aero-engines to produce low pressure turbine blades [1]. Such alloys progressively substitute Ni-based superalloys reducing by the way the weight of parts and increasing the overall efficiency of the engine. Among the different alloys developed in the literature, two main compositions are worked out at industrial scale. The first is the well-known peritectically-solidified Ti-48Al-2Cr-2Nb (Ti-48-2-2), developed in the 80's by General Electrics and optimized for casting. The second is the

beta-solidified Ti-44Al-4Nb-1Mo-0.1B (TNM-B1) alloy, optimized for hot-die forging and developed by Clemens et al. [2]. In service, turbine materials are subjected to long-term oxidation in air, in the 600-700°C range, in conditions of cyclic mechanical solicitation. Therefore, the thermal history of the materials may affect their mechanical strength, in particular concerning fatigue life in this temperature range. In the present study, our objective is then to account for the effect of pre-exposure in air (650-700°C, 500 h), on the fatigue strength at high temperature (633-683°C) of Ti-48-2-2 and TNM-B1 alloys.

Many works have focused on the effect of exposure at high temperature in air, in terms of sub-surface microstructure and of mechanical properties. A review can be found for example in Appel's book [1]. Oxidation processes of TiAl give rise to the following phase sequence in the sub-surface: TiAl – Al depleted zone – TiO_2+Al_2O_3 [3, 4]. The Nb and Mo elements which are added to the TNM-B1 alloy have been found to improve oxidation resistance [5-9]. Nb favors formation of a protective Al_2O_3 layer [5, 7, 9], and Mo has been shown to induce formation of β phase, in which Al diffusion may be fast and O solubility may be low, thus favoring also formation of Al_2O_3 [6]. Concerning the mechanical properties, the effect of exposure at high temperature in air has been shown to induce the striking phenomenon of catastrophic embrittlement at room temperature, that is, strong reduction of ductility [1, 10-15]. This spectacular phenomenon has been accounted for by formation of a brittle surface layer [10], which could be due to O diffusion [14], or by a complex scenario involving oxygen enrichment of a superficial layer, hindering of twinning towards the surface, and influence of near surface stress gradients [15]. Concerning fatigue strength at room temperature, the influence of pre-exposure in air a high temperature (700°C, 10000 h) has been investigated in details for various alloy compositions by Huang et al.: Ti-44Al-5Nb-1W-1B [16, 17], Ti-44Al-8Nb-1B [18], Ti-44Al-4Nb-4Zr-0.2Si-1B [19] and Ti-45Al-2Mn-2Nb-0.8 vol%TiB2 [20]. In these conditions, deterioration of the fatigue strength has been found to be moderate [16, 17], or not significant [18], and fatigue strengthening has even been observed [19, 20]. However, only few studies [14, 21] investigated the impact of oxidation on high temperature fatigue properties, which moreover gave contradictory results. For nearly lamellar microstructures, Draper et al. [14] reported little influence of 800°C air exposure on fatigue strength of specimens tested at room temperature and at 650°C. Conversely, Planck et al. [21] showed that for nearly lamellar alloys, air exposure for 500 h at 760°C reduces fatigue strength by 25%.

Thus, the impact of air exposure on fatigue properties at high temperature is still unclear. Here, we investigate the two emblematic alloys indicated above, the near-γ Ti-48-2-2 and the β-containing TNM-B1 alloys. For this purpose, the materials have been exposed in air at 650-700°C for 500 h. Then, they have been mechanically tested in tension at room temperature, at 673-723°C and in fatigue at 673°C-723°C. To interpret the results, careful microscopic characterizations of the microstructural changes in the near surface have been carried out by SEM and TEM, using in particular the FIB technique to selectively investigate local phase transformations, and the ACOM analysis for phase identification.

2. Experimental

In this study, two sets of specimens were prepared. One was Ti-48Al-2Cr-2Nb at% (Ti-48-2-2) sheets processed by powder metallurgy and was delivered by PLANSEE AG, Austria, in batches of 2 mm of thickness. Pre-alloyed ingots were gas-atomized into spherical powders, subsequently isostatically hot-pressed in the range 1000-1300°C in a rectangular-shaped can. Several rolling passes were then applied to obtain final sheets. Sheets were in primary annealed state, which is obtained typically after a heat treatment of 1000°C for 2h. More details of the sheet rolling process can be found in [22, 23]. The second set of specimens was Ti-43.5Al-4Nb-1Mo-0.1B at% (TNM-B1) sheets processed by hot rolling process from cast ingots and delivered by GfE in batches of 1 mm in thickness. VAR melted and centrifugal casted ingots were subsequently hot rolled with a conventional rolling mill. After a flattening step, sheets were heat treated at a temperature below the γ-solvus temperature. More details of the sheet rolling process can be found in [24]. Starting microstructures for both alloys are shown in Fig. 1.

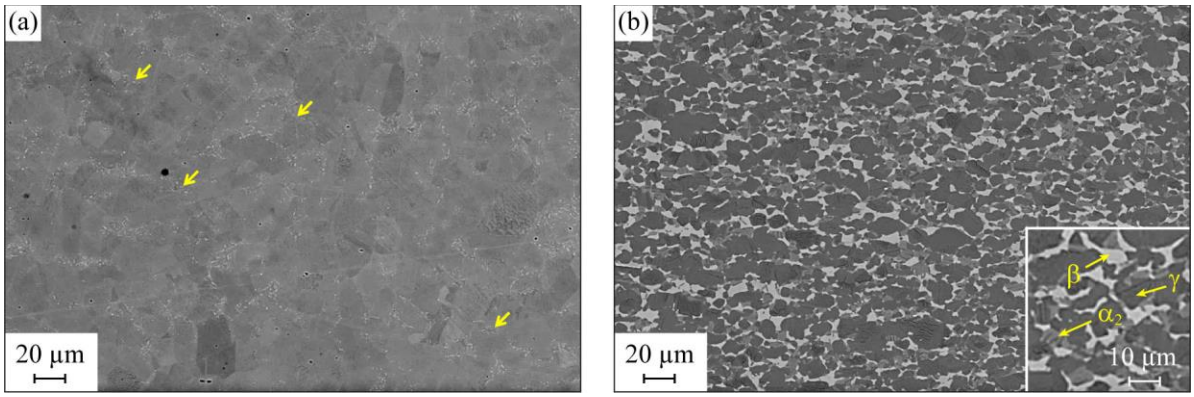

Fig. 1. Starting microstructures of the investigated alloys. (a) Ti-48-2-2 alloy. Arrows indicate Cr-rich phases. (b) TNM-B1 alloy. β, α_2 and γ phases appear in light, medium and dark grey, respectively (see insert).

Due to process parameters, both alloys are in near-γ state. Cr-rich phases can be identified in the Ti-48-2-2 samples which represent less than 0.8% of the volume of material. TNM-B1 alloy contains about 18% of β phase and small amounts of α_2+γ grains. More details on microstructural features of TNM-B1 sheets can be found in Erdely et al.'s work [24]. Average grain size is equivalent in both case and is about 20 µm.

Flat tensile and fatigue specimens were EDM-machined directly from the sheets before testing, with 23 mm and 25 mm gauge lengths, respectively. A circular notch with 1 mm overall notch depth (K_t=1.2, were K_t is the theoretical elastic stress concentration factor) was introduced in fatigue specimens.

After machining and cleaning in acetone, tensile and fatigue specimens were split into three groups. Specimens in Group A were tested directly (no exposure), specimens in Group B and C were exposed individually in air furnace for 500 h at 650°C and 700°C respectively before testing.

Tensile tests were carried out at a constant cross-head speed of 5×10^{-3} min^{-1}, at room temperature, 673 and 723°C. S-N fatigue tests were carried out in air at 633°C on Group B specimens and 683°C on Group C specimens, with a frequency of 50 Hz and a load ratio R of 0.1 (where $R=\sigma_{min}/\sigma_{max}$, σ_{min} and σ_{max} are the minimum and maximum stresses for each fatigue cycle). The maximum number of cycles was set to 10^7 cycles, corresponding to a total test duration of about 56 hours.

Microstructures before and after thermal exposure were analyzed in cross section by scanning electron microscopy (SEM), coupled when necessary with energy-dispersive spectroscopy (EDS). Fine microstructural features were furthermore analyzed using transmission electron microscopy (TEM), with a Jeol 2010 apparatus for conventional imaging, and a CM 20 FEG microscope for characterizations by STEM EDX (local chemistry analyses), and for automated crystal orientation mapping (ACOM) (phase determination). A detailed presentation of the ACOM technique can be found in Ref. [25]. It is based on determination of the phases in the thin foil, by acquisition of diffraction patterns and comparisons with databases. The acquired diffraction patterns were compared with those of the γ, α_2 and B2 phases, which have been determined from crystallographic data of the ICSD database. The acquisitions were carried out with a lateral resolution of 6 nm. For the STEM EDX studies, a pixel size of 14 nm was selected. The procedure for FIB lift out of TEM thin foils has been determined in a preceding study [26], and was also employed here. Fig. 2 shows an example of a FIB lift out experiment on the oxidized surface of TNM-B1 sample (pre-exposed in the conditions 700°C-500 h, group C). Fig. 2a shows the oxidized surface of the material and the thin foil just before extraction. To protect the cross-section from the ion beam close to the surface, Pt deposition has been performed in two steps. Fig. 2b shows the TEM thin foil obtained. The two Pt deposits can be shown on the surface. Below, oxide structured in layers can be seen.

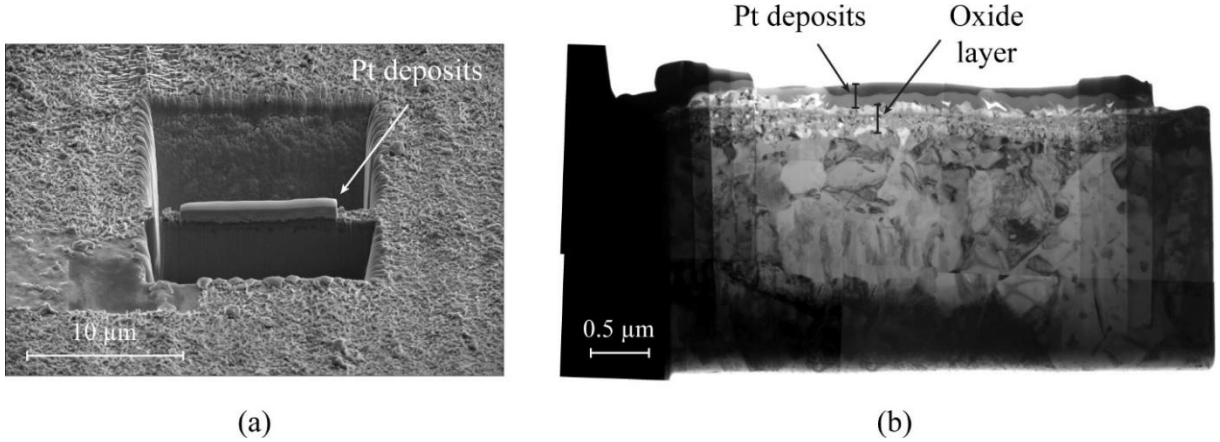

Fig. 2. (a) SEM image taken during the procedure of TEM thin foil extraction by FIB, on the oxidized surface of an exposed (700°C/500 h, group C) TNM-B1 sample. Note the two Pt deposits above the surface. (b) TEM image of the thin foil.

FIB lift-outs have been carried out in the γ and β zones of the TNM-B1 alloy. Extraction in γ zones did not require particular attention, because this phase represents ≈ 80% of the material, and operating randomly proved satisfactory. However, extraction in the β zones, which represents ≈ 20% of the material, required pre-localization by SEM of the zone on cross-sections, and local selective extraction by FIB.

3. Results

3.1. Tensile properties

The results of the tensile tests at room and high temperatures for the two alloys are gathered in Table 1. For γ-Ti-48-2-2, considering measurement scattering, the impact of exposure is not clear at room temperature. Without exposure, plastic elongation is 0.89 % and UTS is 424 MPa. After exposure at 650°C, the ductility seems to remain unaffected (plastic elongation of 0.73%), and after exposure at 700°C, the ductility seems even to increase (plastic elongation of 1.17%), with however a strong scattering of the results, leading to an error of ± 1.2 %. Similarly, the influence of pre-exposition on the high temperature tensile properties does not exhibit any obvious trend: at a testing temperature of 673°C, the ductility changes from 4.8% without exposure to 4.96% after 650°C exposure, and at a testing temperature of 723°C, the ductility changes from 3.24% without exposure, to 2.02 % after 700°C exposure. On the contrary, embrittlement is clearly evidenced for the β-containing TNM-B1 alloy. Thus, at room temperature, plastic elongation drops from 1.04% down to 0.25 % after exposures at 650°C and 700°C for 500 h, reducing at the same time UTS from 880.7 MPa to 420-429.7 MPa. Embrittlement is also observed in tension at high temperature. Hence, for test temperature of 673°C, ductility is reduced from 5.52 % without exposure to 2.15 % after exposure at 650°C, and ductility at 723°C is reduced from 9.5 % without exposure to 3.57 % after exposure at 700°C. These results seem to indicate an influence of the presence of β phase on the embrittlement of TiAl alloys after exposure at 650-700°C for 500 h.

Table 1. Room and high temperature tensile properties of the Ti-48-2-2 and TNM-B1 alloys for various exposure conditions.

Material	Exposure temp. (°C)/time (h)	Test temp. (°C)	UTS (MPa)	Plastic elongation (%)
Ti-48-2-2 - Group A	None	25	424.3 ± 11	0.89 ± 0.2
Ti-48-2-2 - Group B	650/500	25	416.7 ± 5	0.73 ± 0.2
Ti-48-2-2 - Group C	700/500	25	415 ± 3	1.17 ± 1.2
Ti-48-2-2 - Group A	None	673	505.5 ± 9	4.8 ± 0.4
Ti-48-2-2 - Group B	650/500	673	474.5 ± 20	4.96 ± 0.9

Ti-48-2-2 - Group A	None	723	516.5 ± 22	3.24 ± 0.2
Ti-48-2-2 - Group C	700/500	723	496 ± 14	2.02 ± 2.6
TNM-B1 - Group A	None	25	880. 7 ± 18	1.04 ± 0.1
TNM-B1 - Group B	650/500	25	429.7 ± 25	0.25 ± 0.03
TNM-B1 - Group C	700/500	25	420 ± 29	0.25 ± 0.05
TNM-B1 - Group A	None	673	823.7 ± 13	5.52 ± 1
TNM-B1 - Group B	650/500	673	796 ± 2	2.15 ± 0.09
TNM-B1 - Group A	None	723	718 ± 22	9.5 ± 7
TNM-B1 - Group C	700/500	723	739 ± 1	3.57 ± 0.6

3.2. Fatigue properties

Fatigue data obtained on both alloys for the different Groups are presented in Fig. 3. In all cases, to ease comparisons, the maximum fatigue stress has been divided by the UTS measured at 673°C, considering that this value is close to measurements carried out at 633°C and 683°C.

When looking at Ti-48-2-2 alloy, accounting for the rather small amount of specimens tested for each exposure groups and each temperature, all the results seem to follow the same trend. This shows, first, that the test temperature (633°C and 683°C) has little influence on the fatigue properties, as already observed by Sastry et al. [27]. Second, these results indicate that the fatigue properties seem independent of the pre-oxidation conditions.

Concerning TNM-B1 alloy, results from Group A (no high temperature exposure) tested in fatigue at 633°C and 683°C are merged, showing again limited impact of the testing temperature on the fatigue properties. However, contrary to the Ti-48-2-2 alloy, a strong reduction in fatigue strength of the TNM-B1 alloy is observed for groups B and C. This reduction in properties becomes larger when the exposure temperature increases: reductions of 13% for Group B (650°C/500 h), and of 26% for Group C (700°C/500 h) in fatigue strength, are observed. Thus, the fatigue properties observed on the TNM-B1 material seem strongly impacted by pre-exposure, the reduction ratio being significantly dependent on the exposure temperature.

In summary, the test temperature (633°C and 683°C) does not exhibit any noticeable influence on the fatigue strength of the two alloys. On the contrary, pre-exposition in the same temperature range (650°C and 700°C) exhibits a marked influence on the fatigue properties of the β-containing TNM-B1 alloy (drop of fatigue strength up to 26% after 700°C/500 h exposure), but essentially no influence on the 48-2-2 alloy. This result, besides composition differences between both alloys,

seems related to the presence of a large amount of β phase in TNM-B1 compared to 48-2-2. In the following, this working assumption will be evaluated.

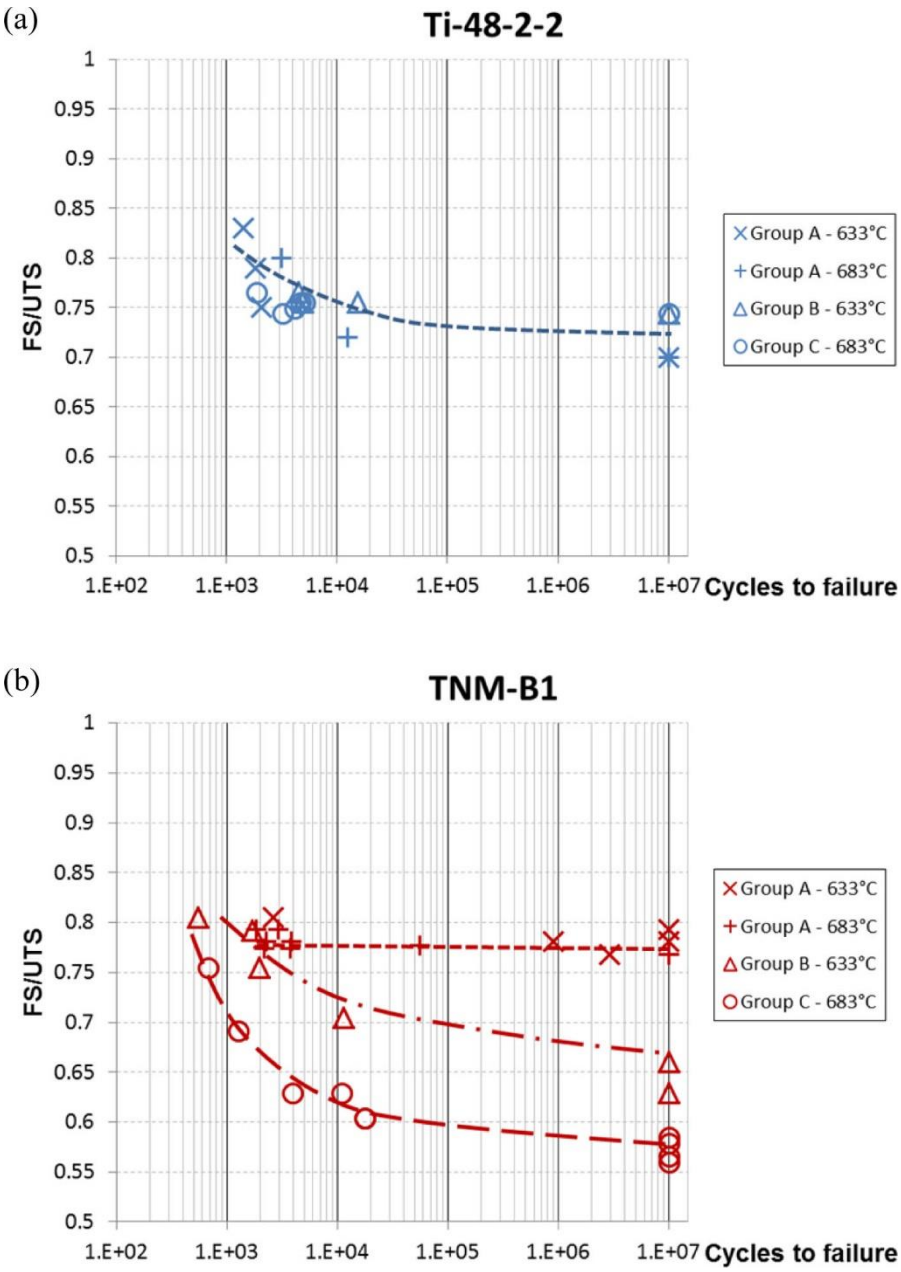

Fig. 3. Fatigue properties for (a) Ti-48-2-2 and (b) TNM-B1 alloys for various exposure conditions.

3.3. Microstructure characterizations

Microstructure characterizations of the near surface modifications due to the high temperature fatigue tests and to the pre-exposition, have been carried out. We have in particular analyzed in more detail the transformations of the β phase, which presence seems to induce embrittlement.

First, the effect of the exposition at high temperature after the fatigue tests (633°C and 683°C for max. 56 h) has been studied by SEM, on samples without pre-exposition (Group A). The results indicate no significant modification of the microstructure close to the surface for both Ti-48-2-2 and TNM-B1 alloys (see the example of TNM-B1 Fig. 4). Thus, in the following, the effect of the exposition at high temperature during the fatigue tests has been neglected.

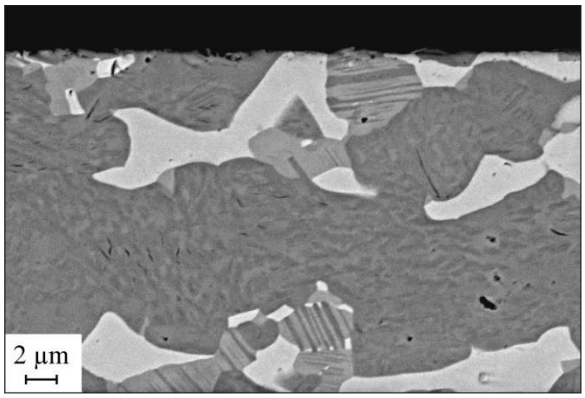

Fig. 4. Surface characterization of TNM-B1 alloy of Group A (no pre-exposition, tested at 633°C/10^7 cycles).

Then, the effect of pre-exposure at high temperature has been investigated. 650°C-500 h (group B) and 700°C-500 h (group C) conditions have thus been investigated. For both TNM-B1 and Ti-48-2-2 alloys, Al_2O_3-TiO_2 oxide layers were formed. However, in the two alloys, the oxide layers were very thin (<1 µm, see the example of a Group C TNM-B1 sample in Fig. 2). Therefore, it can readily be concluded that the difference in embrittlement between the TNM-B1 and Ti-48-2-2 alloys cannot be attributed to these oxide layers, because of their too limited thickness. In other words, it seems that the embrittlement is induced by modifications in the sub-surface below the oxides. We will then in the following concentrate on the characterization of the sub-surface.

For this purpose, cross section analyses of the microstructure, were conducted on both TNM-B1 (Fig. 5a-b) and Ti-48-2-2 (Fig. 6) alloys. In the case of the TNM-B1 alloy, local modifications of the near surface microstructure in the form of lath-like zones, are observed. The width of the affected zone is larger for pre-exposure at 700°C (group C, Fig. 5b) than at 650°C (group B, Fig. 5a). In these two cases, the zone affected by the pre-exposition is somewhat wider in the β regions than in the γ regions. Thus, these results indicate again a potential influence of the β phase on embrittlement, because the zone affected by the pre-exposure is wider in the regions of the sub-surface in which this phase is present. Using these observations, transformation layers in β and γ grains can be measured. Estimated values are summarized in Table 2.

Table 2 Estimated transformed layer thicknesses in γ and β phases

Pre-exposition temperature	650°C	700°C
Transformed layer thickness in γ	1.9 ± 0.5 µm	3.9 ± 0.5 µm
Transformed layer thickness in β	3.8 ± 0.5 µm	6.4 ± 0.5 µm

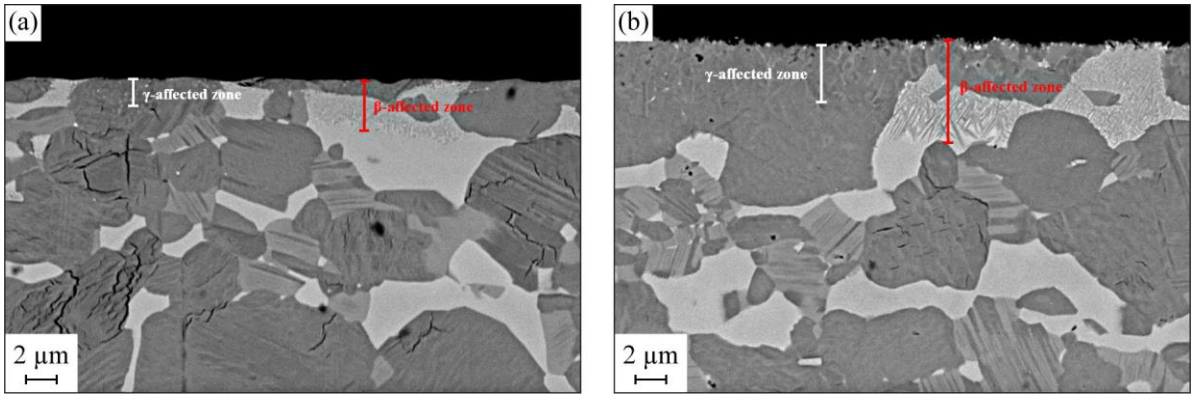

Fig. 5. Surface characterization of TNM-B1 alloy after testing for (a) Group B (650°C/500 h) and (b) Group C (700°C/500 h) specimens. In both case 10^7 cycles have been reached in fatigue.

Conversely, when investigating in the same way the surface of Ti-48-2-2 belonging to Group C, no surface modifications can be detected (Fig. 6).

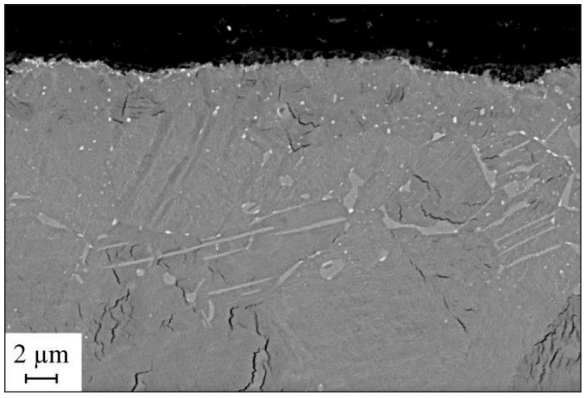

Fig. 6. Surface characterization of a Ti-48-2-2 of Group C (700°C/500 h) specimen after testing.

To study in more details the microstructure modifications in the sub-surface in presence of β phase, TNM-B1 alloys pre-exposed in the harshest conditions (700°C-500 h, group C) have been investigated more accurately, using FIB and TEM techniques. The objective was to investigate finely the transformations occurring in the β phase, in comparison to those taking place in the γ phase.

Thus, FIB thin foil have been randomly extracted in the γ phase of a TNM-B1 sample pre-exposed in the conditions 700°C-500 h (Group C), following the procedure detailed in the experimental section (see Fig. 2). The analyzed region is shown in Fig. 7. It was of about 2 µm in depth, and was therefore completely situated in the zone affected by air exposure. First, a thin oxide layer (< 1 µm) can be identified, as indicated above. Below the oxide layer, diffraction experiments showed that most of the region consisted in γ phase. In this phase, regions labelled 1 about 0.2×0.5 µm in size are characterized by higher Ti, lower Al, and higher O concentrations than the surrounding γ matrix. Diffraction analyses (insert in Fig. 7a) show that these regions are constituted of α_2 phase. Concerning the alloying elements, analyses (not shown) indicate that Mo is roughly homogeneously distributed, whereas Nb seems on the contrary more concentrated in the vicinity of the surface, an effect which has already been reported [28]. To summarize, the effect of air exposure is the formation of α_2 zones in the γ grains of the near surface.

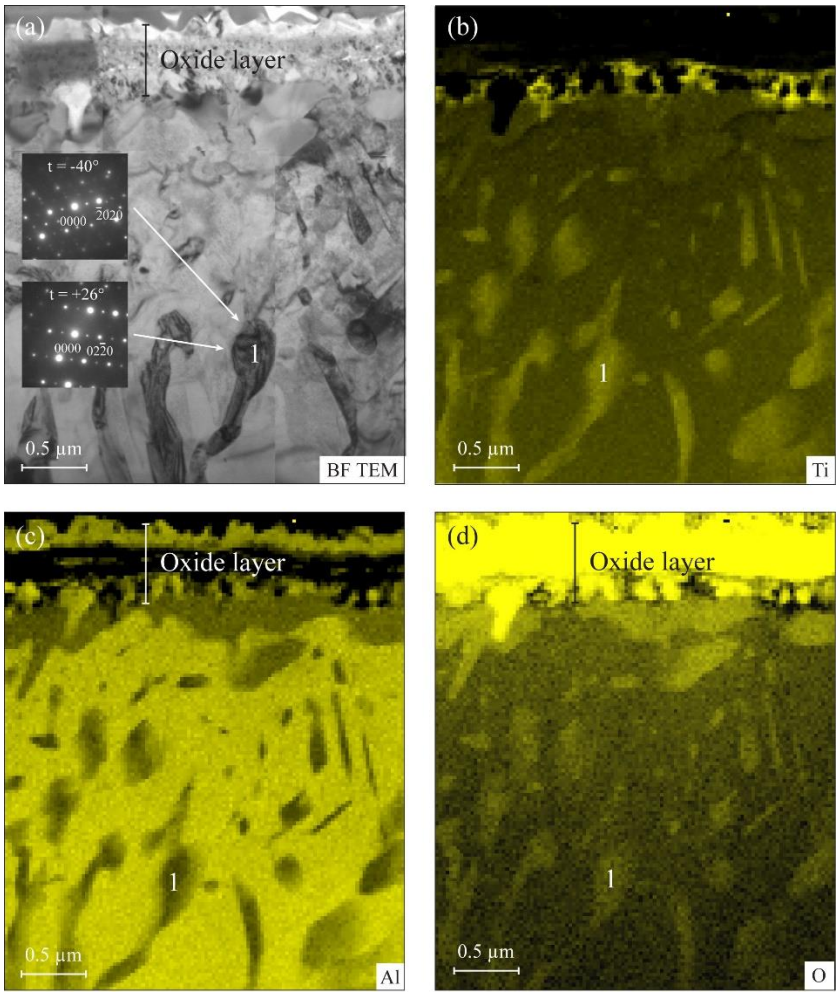

Fig. 7. STEM EDX maps of a γ zone (TEM thin foil extracted by FIB). (a) Bright field TEM image, with diffraction patterns for two tilt (t) angles, allowing to index the crystallographic structure of zone labelled 1 as α_2. (b-d) Ti, Al and O maps, respectively.

Selective investigations of the destabilized β phase in the sub-surface region have also been carried out. Fig. 9 shows STEM-EDX maps of the destabilized β phase. Zones of higher Al concentration, and of lower Ti and O concentration appear. Because of a higher Ti/Al ratio, these zones can be constituted of α_2 or γ phase. Analyses of Nb and Mo (not shown) indicated that Nb concentration was higher in the Al-rich region, and that Mo repartition was more complex, and not readily linked to the repartition of the other elements.

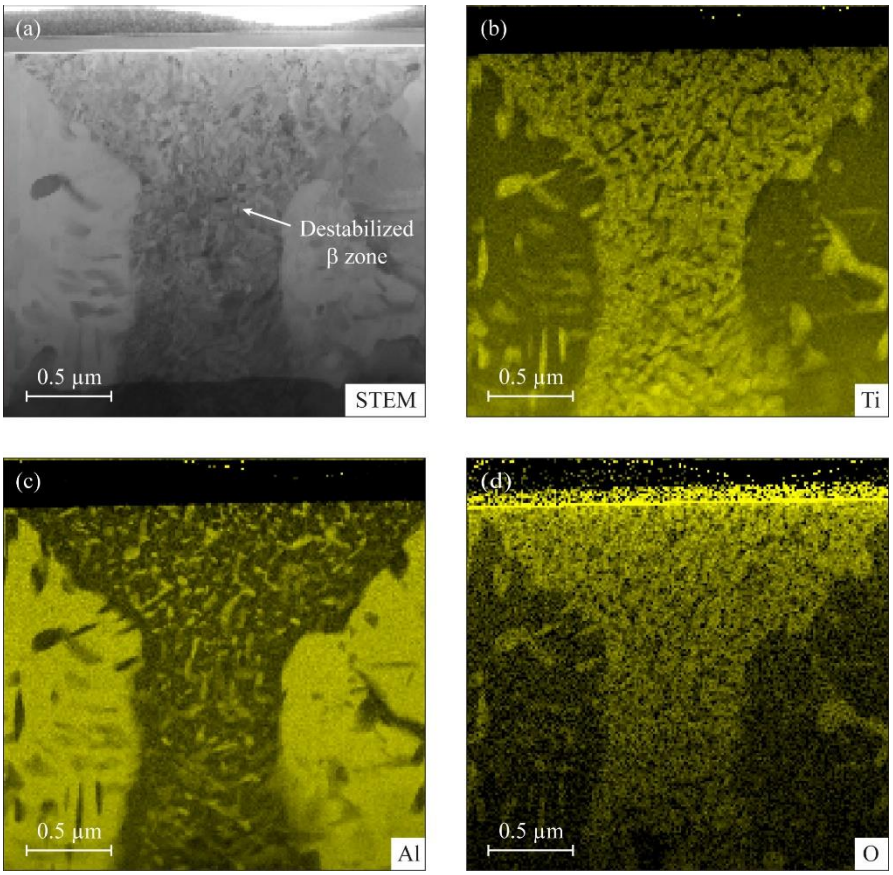

Fig. 8. STEM EDX maps of a destabilized β zone (TEM thin foil extracted by FIB). (a) STEM image. (b-d) Maps of Ti, Al and O.

Fig. 9 shows an ACOM analysis performed in a region of the destabilized β phase shown in Fig. 8. A small area has been analyzed, in order to determine the phase transformations occurring at small scale. It appears that the initial β phase (in green) primarily transforms into α_2 (in blue) and slightly in γ (in red).

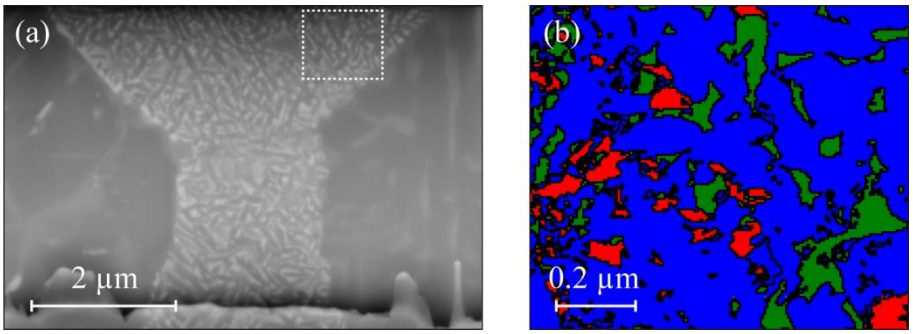

Fig. 9. (a) SEM image of the destabilized β region shown in Fig. 8. (b) ACOM analysis of the region indicated by a rectangle (blue: α_2, green: β, red: γ).

4. Discussion

In this work, loss of ductility at room and high temperatures (Table 1), as well as loss of fatigue strength at high temperature (633-683°C, Fig. 3) of the β-containing TNM-B1 alloy is clearly observed after high temperature pre-exposition (650-700°C, 500 h) in air. Conversely, pre-exposition of the near-γ Ti-48-2-2 alloy does not lead to loss of fatigue strength, and the ductility measurements for this alloy at room and high temperatures after pre-exposure are too scattered to indicate embrittlement unambiguously. Therefore, these results indicate that the β-containing TNM-B1 alloy is more sensitive to embrittlement than the near-γ Ti-48-2-2 alloy. These results point on a probable influence of the presence of the β phase for embrittlement. Moreover, embrittlement of the TNM-B1 alloy is not correlated to variation of tensile strength, which would be the consequence of changes in dislocation mobility due to microstructure modifications in volume (precipitation, increase in dislocation density, etc.). More probable reasons are then microstructure changes in the near surface, as proposed in several studies dealing with room temperature embrittlement of TiAl alloys after high temperature exposure [1, 10-15, 29]. Therefore, we have investigated the sub-surface phenomena occurring in the β phase in the TNM-B1 alloy by SEM and TEM.

SEM investigations showed that, for exposure at 700°C for 500 h, the near surface region of the TNM-B1 alloy, below the oxide layers, undergoes modifications over a thickness of ≈ 4-6 µm (Fig. 5 and Table 2). Both β and γ phases are affected, but the β phase seems to be transformed over a wider thickness than the γ phase. TEM observations of FIB thin foils extracted in the γ phase in near surface region show formation of α_2 zones (Fig. 7a) of low Al and high O concentrations (Fig. 7 c and d). This means diffusion of O towards the bulk and of Al towards the surface. This observation is in agreement with the usual description of the phase sequence in the sub-surface of oxidized TiAl, namely: TiAl – Al depleted zone – TiO_2+Al_2O_3 [3, 4]. Concerning Al, an estimation of the diffusion length d can be carried out using the usual relation $d = 2\sqrt{Dt}$ (with D: self diffusion coefficient and t: time). Using an estimation of the diffusion coefficient at 700°C ($D \approx 6\times10^{-20}$ m^2/s) from the calculations of Herzig *et al.* [30], a value of $d \approx 0.7$ µm is found. This is lower than the length of the affected zone (4-6 µm). This discrepancy is attributed to the limited

accuracy of the diffusion data, especially at low temperatures. The transformation of γ into α_2 can be easily interpreted by the solubility of oxygen into these two phases. It is well reported that the α_2 phase can dissolve high amounts of oxygen: solubilities of 1.9 at. % [31], 14.8 at. % [32], 10-20 at. % [3] are reported. Conversely, the solubility of oxygen in γ, of the order of 200-250 at. ppm [31, 33], is rather limited. Therefore, oxygen probably favors formation of α_2 at the expenses of γ.

In the β phase of the sub-surface, formation of zones of high Al and low O concentrations, is observed (Fig. 8). Moreover, the ACOM analyses show that the β phases transforms into α_2 and slightly into γ (Fig. 9). This can also be interpreted in terms of oxygen solubility in these phases. Concerning the β phase, solubility data for oxygen cannot be found, but concentrations of interstitials as C, N and O of 0.3-0.4 at. % have been reported [34, 35]. The solubility of O into α_2 (between 1.9 at. % and 20 at. % depending on the authors, see above) is then much higher than into the β phase. Consequently, transformation of β into α_2 can be accounted for by an influence of oxygen. However, the formation of slight amounts of γ phase is more surprising, because the solubility of oxygen in this phase is low (200-250 at. ppm), as recalled above.

Destabilization of the γ and β phases results then probably from oxygen diffusion. The fact that this destabilization occurs over a wider zone in β than in γ, as observed in Fig. 5, results then probably from higher O diffusion coefficient in β than in γ. Unfortunately, only few data exist on diffusion of O in the different phases of the TiAl alloys. Experimental data can be found for diffusion of O in α_2 [32, 36], with some discrepancy. At 800°C for example, values of $4\text{-}6\times10^{-18}$ m^2/s [36] and 1.1×10^{-16} m^2/s [32], are reported. Diffusion coefficient of O in γ-TiAl is unknown, probably because of the very limited solubility. However, measurements were carried out in amorphous TiAl and in crystalline Ti_3Al layers deposited in sputtering experiments [37]. In both cases, close values of oxygen diffusion coefficients ($\approx 10^{-14}$ m^2/s at 700°C), were obtained. But, as indicated in the paper, diffusion coefficient in crystalline γ-TiAl would most probably be lower. Finally, the diffusion coefficient of O in the β phase has also not been measured. An order of magnitude could be the value obtained for diffusion of O in β Ti, which at 800°C is $2\text{-}5\times10^{-12}$ m^2/s, and at 700°C would be (by extrapolation of the existing data) $2\text{-}5\times10^{-13}$ m^2/s [38]. Thus, in this case, the diffusion coefficient at 800°C of O in β would be significantly more elevated than in α_2 and γ.

To compare with these results, we have used the data from Table 2 to estimate oxygen diffusion coefficients at 700°C in the γ and β phases, assuming that the reaction kinetics is controlled by oxygen diffusion. Values in the range $2\text{-}3\times10^{-18}$ m^2/s for γ and $5\text{-}7\times10^{-18}$ m^2/s for β are found. These values seem to be significantly lower than that given in Refs. [37], for O diffusion in amorphous TiAl, and in Ref. [38], for O diffusion in β Ti. In spite of these discrepancies, which remain to be better understood by diffusion investigations, our experimental studies clearly indicate the influence of oxygen diffusion in the destabilization of the surface layer.

5. Conclusions

Near-γ Ti-48Al-2Cr-2Nb (Ti-48-2-2) and β-containing Ti-44Al-4Nb-1Mo-0.1B (TNM-B1) alloys have been mechanically tested in tension at room temperature and in fatigue at 633-683°C after pre-exposure in air at high temperature (650-700°C, 500 h). No obvious effect of the pre-exposure on ductility at room temperature and at 673-723°C of the Ti-48-2-2 alloy has been observed. On the contrary, clear embrittlement has been found for the TNM-B1 alloy: drop of ductility at room temperature from 1.04% to 0.25 % and of ductility at 723°C from 9.5 % to 3.57 %, have been measured after pre-exposures (650-700°C, 500 h). In fatigue, varying the test temperature (633°C and 683°C) did no exhibit noticeable influence on the fatigue strength of the two alloys. But again, pre-exposure (650-700°C, 500 h) exhibited a marked influence on the fatigue properties at 633-683°C of the β-containing TNM-B1 alloy (drop of fatigue strength up to 26%), but essentially no influence on the 48-2-2 alloy. Sub-surface microstructure exhibited marked evolutions in the β-containing TNM-B1 alloy, whereas no evolution was observed in the γ-Ti-48-2-2 alloy, pointing on a potential impact of these sub-surface evolutions, and on the presence of β phase, on the embrittlement phenomenon. First attempts to characterize these sub-surface evolutions have been carried out by SEM, EDX-TEM and ACOM investigations, using the FIB technique to locally extract TEM thin foils in γ and β regions of the sub-surface. It has been observed that the γ and β phases are destabilized according to $\gamma \rightarrow \alpha_2$ and $\beta \rightarrow \alpha_2 + \gamma$ transformations, O diffusion from the surface inducing formation of high solubility α_2 phase. Moreover, the wider extension of the destabilized zone in β than in γ is interpreted by a probable higher diffusion coefficient of O in β than in γ.

References

[1] F. Appel, J. Paul, M. Oehring, Gamma titanium aluminide alloys, Wiley, Weinheim, 2011.

[2] H. Clemens, S. Maier. Design, processing, microstructure, properties, and application s of advanced intermetallic TiAl alloys, Advanced Engineering Materials 15 (2013) 191-215.

[3] A. Rahmel, W.J. Quadakkers, M. Schutze, Fundamentals of TiAl oxidation - A critical review, Materials and Corrosion 46 (1995) 271-285.

[4] J. Malecka, Transformation and precipitation processes in a metal substrate of oxidized TiAl-based alloys, Oxidation of Metals 91 (2019) 365-380.

[5] K. Maki, M. Shioda, M. Sayashi, T. Shimizu, S. Isobe, Effect of silicon and niobium on oxidation resistance of TiAl intermetallics, Materials Science and Engineering, A153 (1992) 591-596.

[6] Y. Shida, H. Anada, The influence of ternary element addition on the oxidation behaviour of TiAl intermetallic compound in high temperature air, Corrosion Science 35 (1993) 945-953.

[7] B.G. Kim, G.M. Kim, C.J. Kim, Oxidation behavior of TiAl-x (x = Cr, V, Si, Mo or Nb) intermetallics at elevated temperature, Scripta Metallurgica et Materialia 33 (1995) 1117-1125.

[8] H. Nickel, N. Zheng, A. Elschner, W.J. Quadakkers, The oxidation behaviour of niobium containing γ-TiAl based intermetallics in air and argon/oxygen, Mikrochimica Acta 119 (1995) 23-39.
[9] M. Yoshihara, K. Miura, Effects of Nb addition on oxidation behavior of TiAl, Intermetallics 3 (1995) 351-363.
[10] W.E. Dowling, W.T. Donlon, The effect of surface film formation from thermal exposure on the ductility of Ti-48Al-1V-0.2C, Scr. Metall. Mater. 27 (1992) 1663.
[11] C.M. Austin, T.J. Kelly, Structural intermetallics. TMS, Warrendale, 1993.
[12] T.J. Kelly, C.M. Austin, P.J. Fink, J. Schaeffer, Effect of elevated temperature exposure on cast gamma titanium aluminide (Ti-48Al-2Cr-2Nb). Scr. Metall. Mater. 30 (1994) 1105.
[13] S.K. Planck, A.H. Rosenberger, Gamma titanium aluminides, TMS, Warrendale, 1999.
[14] S. Draper, B. Lerch, I. Locci, M. Shazly, V. Prakash, Effect of exposure on the mechanical properties of Gamma MET PX, Intermetallics 13 (2005) 1014-1019.
[15] M. Thomas, O. Berteaux, F. Popoff, M.P. Bacos, A. Morel, B. Passilly, V. Ji, Effects of exposure at 700°C on RT tensile properties in a PM γ-TiAl alloy, Intermetallics 14 (2006) 1143.
[16] Z. Huang, J. Lin and B. Feng, Microstructural characterization and fatigue response of alloy Ti-46Al-5Nb-1W with varied surface quality and thermal exposure history, Materials Characterization 130 (2017) 285-297.
[17] Z. Huang, J. Lin, Z. Zhao, H. Sun, Fatigue response of a grain refined TiAl alloy Ti-44Al-5Nb-1W-1B with varied surface quality and thermal exposure history, Intermetallics 85 (2017) 1-14.
[18] Z. Huang, T. Cong, Microstructural instability and embrittlement behaviour of an Al-lean, high-Nb gamma-TiAl-based alloy subjected to a long-term thermal exposure in air, Intermetallics 18 (2010) 161-172.
[19] Z. Huang, C. Sun, On the role of thermal exposure on the stress controlled fatigue behaviour of a high strength titanium–aluminum alloy, Materials Science & Engineering A 615 (2014) 29-41.
[20] Z. Huang, S. Huang, On the role of thermal exposure on the stress controlled fatigue behaviour of an intermediate strength γ-TiAl based alloy, Materials Science & Engineering A 636 (2015) 77-90.
[21] S. Planck, A. Rosenberger, The influence of high temperature exposure on the mechanical performance of a gamma titanium aluminide alloy, Materials Science and Engineering A 325 (2002) 270-280.
[22] H. Clemens, P. Schretter, K. Wurzwallner, A. Bartels, C. Koeppe, Forging and rolling of Ti-48Al-2Cr in industrial scale, Warrendale: TMS, 1993.
[23] H. Clemens and H. Kestler, Processing and applications of intermetallic γ-TiAl-based alloys, Advanced Engineering Materials 2 (2000) 551-570.
[24] P. Erdely, P. Staron, E. Maawad, N. Schell, J. Klose, H. Clemens, S. Mayer, Design and control of microstructure and texture by thermomechanical processing of a multi-phase TiAl alloy, Materials and Design 131 (2017) 286-296.

[25] E.F. Rauch, J. Portillo, S. Nicolopoulos, D. Bultreys, S. Rouvimov, et al., Automated nanocrystal orientation and phase mapping in the transmission electron microscope on the basis of precession electron diffraction, Zeitschrift für Kristallographie 225 (2010) 103-109.
[26] Z. Trzaska, A. Couret, J.P. Monchoux, Spark plasma sintering mechanisms at the necks between TiAl powder particles, Acta Materialia 118 (2016) 100-108.
[27] S. M. L. Sastry, H. A. Lipsitt, Fatigue deformation of TiAl base alloys, Metallurgical Transactions A 8 (1977) 299-308.
[28] S. Becker, A. Rahmel, M. Schorr, M. Schütze, Mechanism of isothermal oxidation of the intermetallic TiAI and of TiAl alloys, Oxidation of Metals 38 (1992) 425-464.
[29] J.D.H. Paul, M. Oehring, F. Appel, F. Pyczak, Depth resolved near-surface residual stresses in γ-based TiAl before and after high-temperature exposure, Intermetallics 84 (2017) 103-111.
[30] C. Herzig, T. Przeorski, and Y. Mishin, Self-diffusion in gamma-TiAl: an experimental study and atomistic calculations, Intermetallics 7 (1999) 389-404.
[31] A. Denquin, S. Naka, A. Huguet, A. Menand, Scripta Metallurgica et Materialia 28 (1993) 1131-1136.
[32] S.L. Draper, D. Isheim, Environmental embrittlement of a third generation γ TiAl alloy, Intermetallics 22 (2012) 77-83.
[33] A. Menand, A. Huguet, A. Nérac-Partaix, Interstitial solubility in γ and α_2 phases of TiAl-based alloys, Acta Materialia 44 (1996) 4729-4737.
[34] T. Klein, M. Schachermayer, F. Mendez-Martin, T. Schöber, B. Rashkova, H. Clemens, S. Mayer, Carbon distribution in multi-phase γ-TiAl based alloys and its influence on mechanical properties and phase formation, Acta Materialia 94 (2015) 205–213.
[35] T. Klein, H. Clemens, S. Mayer, Advancement of compositional and microstructural design of intermetallic γ-TiAl based alloys determined by atom probe tomography. Materials 9 (2016) 755.
[36] Y. Koizumi , M. Kishimoto , Y. Minamino, H. Nakajima, Oxygen diffusion in Ti_3Al single crystals, Philosophical Magazine 88 (2008) 2991-3010.
[37] A. Zalar, J. van Lier, E. J. Mittemeijer, J. Kovac, Interdiffusion at TiO_2/Ti, TiO_2/Ti_3Al and TiO2/TiAl interfaces studied in bilayer structures, Surface and Interface Analysis 34 (2002) 514-518.
[38] H. Mehrer (Ed.), Landolt-Börnstein, numerical data and functional relationships in science and technology, group III – vol. 26: diffusion in solid metals and alloys, Springer, Berlin, 1990.